



## City Research Online

### City, University of London Institutional Repository

---

**Citation:** Jebri, B., Phillips, M. L., Knapp, K., Appelboam, A., Reuben, A. & Slabaugh, G. (2015). Detection of degenerative change in lateral projection cervical spine x-ray images. Progress in Biomedical Optics and Imaging - Proceedings of SPIE, 9414, 941404. doi: 10.1117/12.2082515

This is the accepted version of the paper.

This version of the publication may differ from the final published version.

---

**Permanent repository link:** <https://openaccess.city.ac.uk/id/eprint/17435/>

**Link to published version:** <https://doi.org/10.1117/12.2082515>

**Copyright:** City Research Online aims to make research outputs of City, University of London available to a wider audience. Copyright and Moral Rights remain with the author(s) and/or copyright holders. URLs from City Research Online may be freely distributed and linked to.

**Reuse:** Copies of full items can be used for personal research or study, educational, or not-for-profit purposes without prior permission or charge. Provided that the authors, title and full bibliographic details are credited, a hyperlink and/or URL is given for the original metadata page and the content is not changed in any way.



# Detection of Degenerative Change in Lateral Projection Cervical Spine X-ray Images

Beyrem Jebri<sup>a</sup>, Michael Phillips<sup>b</sup>, Karen Knapp<sup>c</sup>,  
Andy Appelboam<sup>d</sup>, Adam Reuben<sup>d</sup>, Greg Slabaugh<sup>\*b</sup>

<sup>a</sup>ENSIIE, 1 Rue de la Resistance, 91000 Evry, France;

<sup>b</sup>City University London, Northampton Square, London, UK;

<sup>c</sup>University of Exeter, Devon, UK;

<sup>d</sup>Royal Devon and Exeter Hospital, Barrack Road, Devon, UK

## ABSTRACT

Degenerative changes to the cervical spine can be accompanied by neck pain, which can result from narrowing of the intervertebral disc space and growth of osteophytes. In a lateral x-ray image of the cervical spine, degenerative changes are characterized by vertebral bodies that have indistinct boundaries and limited spacing between vertebrae. In this paper, we present a machine learning approach to detect and localize degenerative changes in lateral x-ray images of the cervical spine. Starting from a user-supplied set of points in the center of each vertebral body, we fit a central spline, from which a region of interest is extracted and image features are computed. A Random Forest classifier labels regions as degenerative change or normal. Leave-one-out cross-validation studies performed on a dataset of 103 patients demonstrates performance of above 95% accuracy.

**Keywords:** Cervical Spine, Degenerative Change, Spondylosis, Random Forest

## 1. INTRODUCTION

Cervical spondylosis, or arthritis of the neck, is a common condition affecting up to two out of three people in their lifetime.<sup>1,2</sup> It normally results from degenerative changes<sup>3</sup> that occur to the cervical spine (consisting of the topmost seven vertebrae, labeled C1 to C7), as a person ages. Between each vertebral body is an intervertebral disc that provides cushioning between adjacent vertebrae. Due to arthritis, the disc can deflate and weaken, resulting in a loss of spacing between vertebrae. With reduced cushioning, the joints experience greater forces and begin to degenerate, and the cartilage that protects them is worn down. Osteophytes, or bony outgrowths, commonly develop in response to lost cartilage.

Standard procedure to diagnose cervical spondylosis involves a physical exam, which may be followed by additional tests, typically imaging. X-ray radiography is traditionally ordered as a first step in imaging the spine, due to its widespread availability, and low cost. Additional exams including computed tomography (CT), magnetic resonance (MR), and electromyography are also possible. In a lateral radiograph, degenerative changes often appear as vertebral bodies with poor edge definition and limited spacing between vertebrae; examples of a normal spine and those exhibiting degenerative changes are shown in Figure 1.

In this paper we present an algorithm to detect degenerative change based on image analysis techniques applied to x-ray images of the cervical spine. We focus on the lateral projection, the most diagnostic of the three images (lateral, odontoid, and anteroposterior) normally taken in clinical practice. Our objective is to determine which patients have degenerative change, and localize the degenerative change between different adjacent vertebrae in the image (e.g., going from C5 to C6, denoted as “C5/C6”). Our approach uses splines to model a path through the vertebral bodies, and extracts image features, which are then classified using machine learning to output a label (degenerative change, or normal). As a byproduct of our method, we also identify superior and inferior vertebral body edges.

---

\*gregory.slabaugh.1@city.ac.uk; telephone: +44 (0)207 040 8416

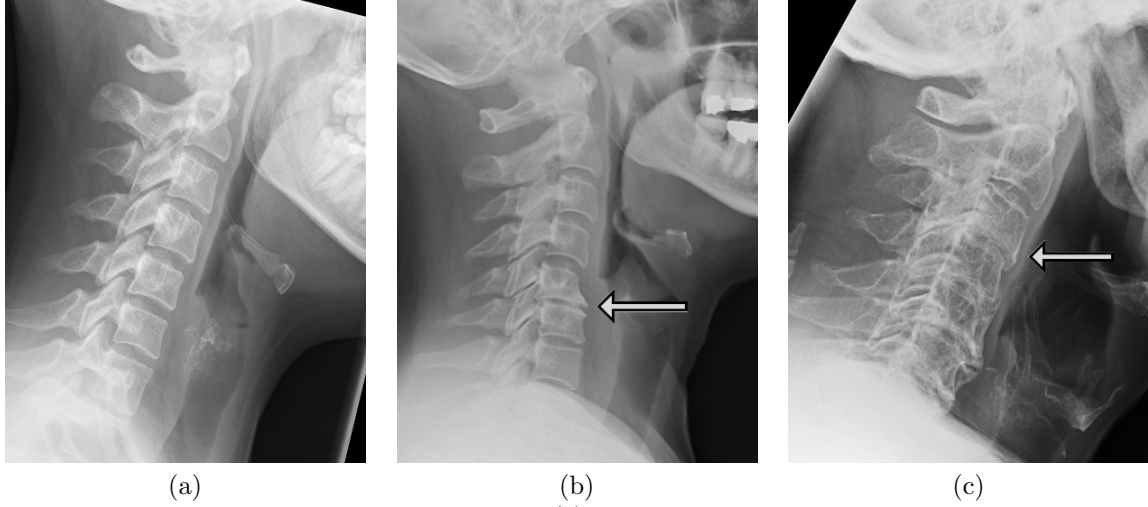


Figure 1. Three lateral view cervical spine radiographs. In (a), a normal cervical spine x-ray image of a 20 year old patient is shown; notice the separation between vertebral bodies and good contrast at vertebral body edges. In (b), an image of a 55 year old patient is shown, with an example of degenerative change (poor vertebrae spacing, osteophyte) indicated. In (c), an example of an 82 year patient with severe degenerative changes is shown; note the lack of identifiable superior and inferior vertebral boundaries as well as vertebral spacing, for example at the point indicated by the arrow.

### 1.1 Related work

Images can be assessed visually for diagnosis of degenerative changes, as well as injuries such as fractures or misalignment. The Atlas of Standard Radiographs of Arthritis<sup>4</sup> defines five numeric grades of severity of degenerative change, ranging from 0 (normal) to 4 (severe), which can be established by consensus for a set of human image readers, but can be difficult to establish accurately given the subtle differences between grades.<sup>13</sup> Quantitative measurements can also be produced manually to capture disc height, vertebral height, and alignment angles<sup>5</sup> using computer-assisted measurement tools available in most workstation software.

Semi-automated image analysis to study osteoarthritis in the spine have been proposed by several researchers. Cherukuri et al.<sup>6</sup> use convex hull-based features in conjunction with a multi-layer perceptron to detect osteophytic vertebral bodies in the lumbar spine given vertebral body segmentation. Abu-Qasmieh<sup>7</sup> detects intervertebral disc degeneration in MR images of the lumbar spine using texture features and a decision tree classifier. Similarly, computer-aided diagnosis of lumbar disc pathology for MR images of the lower spine has been presented.<sup>8</sup> More broadly, there has been work on identification of classification of cervical spine vertebrae,<sup>9</sup> content-based image retrieval based on inter-vertebral disc space and shape profiles,<sup>10</sup> as well as segmentation of cervical vertebrae from radiographic images,<sup>11</sup> all based on radiographic images, in particular the NHANES<sup>12</sup> data set. Since many of these techniques require a precise segmentation of the vertebral bodies, they would fail to produce usable results if presented with a patient with severe degenerative changes.

The most related paper to this work is by Chamrathy et al.,<sup>13</sup> who studied a similar problem of detecting degenerative change in the C3 to C6 vertebrae from cervical spine radiographs. This method requires the user to provide a precise manual segmentation of each vertebral body, from which distance features are computed, clustered, and then classified using a self-organising map. Classification into four grades produced results ranging from 82% to 94%. In contrast, our approach only requires a click at the center of each vertebral body, instead of a precise manual segmentation, and is therefore easier to use. Furthermore, our method is applicable to the entire cervical spine as it does not require a precise segmentation, which can be difficult particularly for the C1 and the superior vertebral body edge of the C2 vertebra, or for patients with severe degenerative changes. Given the ambiguity of assigning the grading criteria to assess the severity of degenerative change, we instead approach degenerative change detection as a binary problem by classifying the space between different adjacent vertebrae as normal or degenerative.

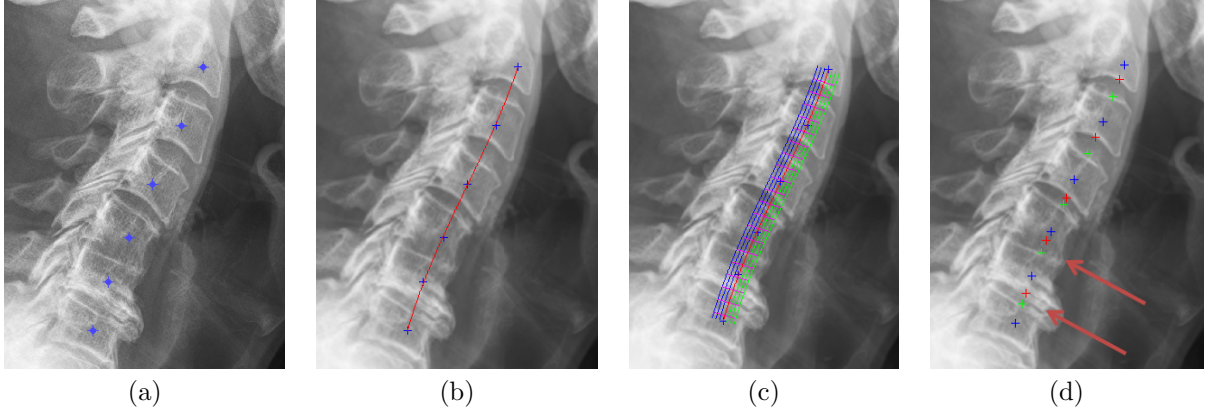


Figure 2. Algorithmic steps. A set of points (a) defining the vertebral body centers is fit to a spline (b). A set of displaced splines are found (c), and the image intensity is resampled along these splines and averaged.  $L = 3$  in this figure for clarity; however, in the experiments we use  $L = 30$ . In (d), the resulting average signal is analyzed to find vertebral body edges (superior: green, inferior: red) and detect degenerative change (arrows).

The proposed method could be easily adapted to other parts of the spine (thoracic, lumbar) or other projections (odontoid, anteroposterior), however, it is beyond the scope of this paper to present results for these applications.

## 2. METHODOLOGY

### 2.1 Signal modeling

The first step of our approach is to fit a third-order spline<sup>14</sup> (called the *central spline* (CS) in this paper) to a set of points located in the center of each vertebral body. These points can be provided by a user in the form of user clicks (our approach in this paper), or detected automatically using pattern recognition techniques. An example set of points is shown in Figure 2(a), and the CS in (b). Our goal is to detect degenerative changes for the region between each click point.

Next, the image is filtered using a zero-mean 2D Gaussian low pass filter with standard deviation 1.8 pixels. The image intensities are then resampled along the CS to form a 1D signal. In the results presented later in the paper, we call this method *CS only*. However, we observed improved results by averaging the signal for  $L$  adjacent splines to the right, and  $L$  to the left, by translating the points in a direction orthogonal to the CS, forming a set of  $2L + 1$  splines, along which the image intensity was resampled. An example showing a subset of these adjacent splines is provided in Figure 2(c). This produces a collection of  $2L + 1$  1D signals, which are averaged to produce a composite 1D signal. In the results below we call this method *averaging*. The 1D signal, whether CS only or averaged, is denoted as  $x(t)$ . To better handle differing contrast in the dataset due to exposure and patient size, we normalize  $x(t)$  as  $x_n(t) = \frac{x(t) - \mu}{\sigma}$ , where  $\mu$  is the mean of  $x(t)$ , and  $\sigma$  is its standard deviation.

### 2.2 Part formation

We first decompose  $x_n(t)$  into a set of parts,  $p_i(t)$ , as shown in Figure 3(b). Part formation is trivial given the user click points input to the approach. The goal of our work then is to automatically classify each part as normal or degenerative change. Each part starts in a vertebral body, transitions through the intervertebral disc region (if present), and then traverses through the adjacent vertebral body. Intuitively, since the vertebral bones are denser than the intervertebral discs, we expect the signal  $p_i(t)$  to have a pattern: brighter, darker, brighter for a normal patient. The darker region, spanning the intervertebral disc region, should have sufficient width, and for a normal patient we expect be good image contrast transitioning between vertebral bodies and the intervertebral disc region. An example  $p_i(t)$  for a normal part is shown in Figure 4(a).

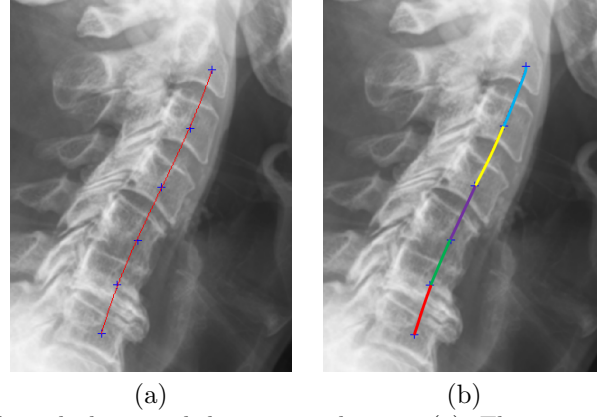


Figure 3. Parts. The spline fit through the user click points is shown in (a). The region between each click point is called a *part* in this paper. In (b), each part is rendered with a different color. Our method classifies each part is normal or degenerative change.

### 2.3 Segmentation

For each part, we first apply a 1D segmentation that produces a signal  $s_i(t)$  formed of three piece-wise constant segments as shown in Figure 4 (b). In this figure, the signal  $p_i(t)$  is shown as the blue signal, and the segmentation  $s_i(t)$  is rendered as a set of horizontal red line segments, each capturing the average intensity of the signal over its domain. Intuitively, as the vertebral body is denser than the intervertebral region, we expect the segmentation to have a higher value in the vertebral body region, and a lower value in the intervertebral region. We also expect a pattern of alternating high, low, and high values in the segmentation, as  $t$  moves between vertebrae.

The segmentation is achieved based on the derivative  $\frac{dp_i(t)}{dt}$ . At the transition  $t_l$  into the intervertebral disc region, we expect the signal intensity to go from brighter to darker, to produce a large negative derivative. Similarly, at the transition  $t_r$  into the next vertebral body region, we expect the signal intensity to go from darker to brighter, to produce a large positive derivative. We detect  $t_r$  as the location of the maximum of  $q_i(t) = w(t) \frac{dp_i(t)}{dt}$ , where  $\frac{dp_i(t)}{dt}$  is computed discretely using a central difference approximation. We then detect  $t_l$  as the location of the minimum of  $q_i(t)$ , for  $t \in [0, t_r]$ . The term  $w(t)$  is a weighting designed to favor selecting transition points near the center of  $p_i(t)$ , near the intervertebral disc. We model  $w(t)$  as a Gaussian function with mean  $N/2$  and standard deviation  $N/4$ , where  $N$  is the length of the part. We refer to  $t_l$  and  $t_r$  as *transition points* for the segment.

As a result of this segmentation, we detect the superior and inferior vertebral body edges. Examples are shown in Figure 2(d), where the superior edge is rendered as a green “+” and the inferior edge is rendered as a red “+”.

### 2.4 Feature extraction

For each part, we extract a total of seven features, denoted  $f_1 \cdots f_7$ , designed to capture degenerative change if present in the part.

The first three features are based on the part’s segmentation,  $s_i(t)$ . Feature  $f_1$  measures the length of the intervertebral region, as demonstrated in Figure 5. Intuitively, we expect normal patients to have larger separation between vertebrae, and consequently a higher  $f_1$  feature compared to those with degenerative change. Features  $f_2$  and  $f_3$  measure the change in intensity level, based on the segmentation, at the transition points  $t_l$  and  $t_r$  respectively. These features are also depicted in Figure 5.

The remaining four features provide different measures of the derivative. Feature  $f_4$  is simply the normalized sum of the absolute value of the two derivatives of  $p_i(t)$  at the transition points, that is

$$f_4 = \frac{\left| \frac{dp_i(t)}{dt} \right|_{t=t_l} + \left| \frac{dp_i(t)}{dt} \right|_{t=t_r}}{\mu}, \quad (1)$$

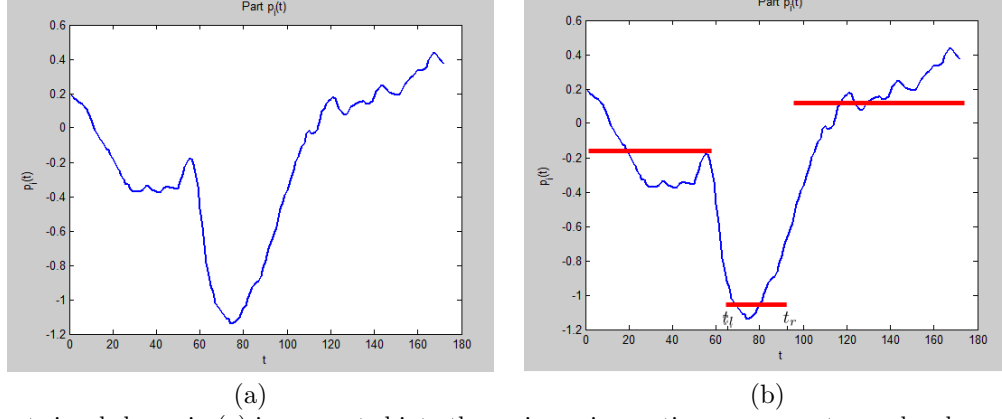


Figure 4. A part signal shown in (a) is segmented into three piece-wise continuous segments, rendered as red lines in (b).

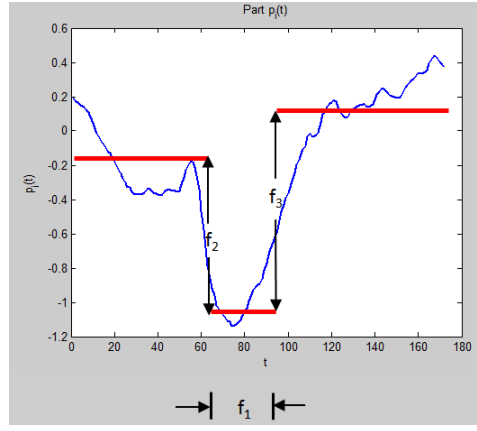


Figure 5. Segmentation features  $f_1$  to  $f_3$ . Feature  $f_1$  measures the length of the intervertebral region. Features  $f_2$  and  $f_3$  measure change in intensity, based on the segmentation, at the transition points.

where  $\mu$  is the mean of  $\left| \frac{dp_i(t)}{dt} \right|$  computed of the length of the part.

Feature  $f_5$  is the unnormalized sum of the absolute value of  $q_i(t)$  at the transition points, that is

$$f_5 = |q_i(t_l)| + |q_i(t_r)|. \quad (2)$$

Feature  $f_6$  is defined as

$$f_6 = \left( \int \left| \frac{dp_i(t)}{dt} \right| dt \right) - \left| \frac{dp_i(t)}{dt} \right|_{t=t_l} + \left| \frac{dp_i(t)}{dt} \right|_{t=t_r}. \quad (3)$$

This feature measures the magnitude of the derivative over the length of the part, but subtracts the magnitude of the derivative at the transition points. For a part with consistent intensity in the vertebrae and intervertebral disc region,  $f_6$  would be small. However, if the signal fluctuates at points other than the transition points, then  $f_6$  will be larger.

The transition points capture the maximum positive and negative derivative of  $p_i(t)$ . However, at a transition point, the intensity change may be gradual instead of a step function. Indeed, in Figure 5 one can see a gradual decrease in brightness at  $t_l$  and a gradual increase at  $t_r$ . To better address gradual brightness changes, we look at the sign of the derivative. For example, at  $t_l$ , we know the derivative is negative, and starting from this point, we decrease  $t$  until we find a point where the derivative becomes positive. Similarly, starting from  $t_l$ , we increase  $t$  until we find a point where the derivative becomes positive. These are denoted using the green points

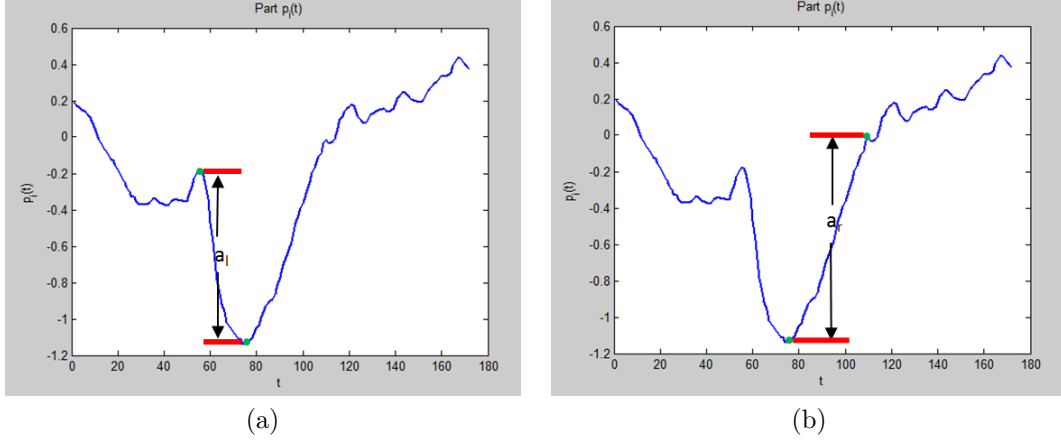


Figure 6. Left (a) and right (b) amplitudes estimated by determining sign changes in the derivative of  $p_i(t)$ . The sum of these amplitudes gives feature  $f_7$ . The points where the derivative sign changes closest to the transition point are rendered in a green color.

in Figure 6 (a). We measure the left amplitude  $a_l$  as the vertical distance between these two points. The right amplitude  $a_r$  shown in Figure 6 (b) is computed in a similar way, by sliding left and right from  $t_r$  to find where the derivative becomes negative.

Feature  $f_7$  is then

$$f_7 = a_l + a_r. \quad (4)$$

The set of features is extracted over the part formed between vertebral body centers, i.e., C1/C2, C2/C3,  $\dots$  C5/C6. We omit the C6/C7 part as our dataset had a number of images where this part was not visible.

## 2.5 Classification

As the cervical spine has a changing appearance along its length, we train a separate classifier for each region. In this paper, we experiment with a kNN classifier ( $k = 3$ , which gave the best results) and a Random Forest (RF) classifier. Leave-one-out cross-validation was performed so that the data used to train the classifier was different from that used to train the classifier. We also perform an experiment comparing averaging the 61 signals vs. using the signal from the CS only, as mentioned earlier.

## 3. RESULTS

We tested our approach on a cohort of 103 patients, with ages ranging from 19 to 96, who had experienced trauma or had symptoms requiring cervical spine radiographs. Patients with post-surgery implants were excluded from this study due to metal plates in their cervical spine. The presence of degenerative change was provided by an expert radiographer, reinforced by radiological reports. Images were acquired subject to ethics approval protocols at the donating institution.

The classification results are presented in Table 1. As the results were produced using a leave-one-out cross-validation, the values in the table show an average over 103 runs, each time holding one sample out, training the classifier, and testing the classifier using the held-out sample. Random Forest was observed to have improved performance compared to kNN. The best results for each part, in terms of accuracy, sensitivity, and specificity appear as bold in the table. Generally, the averaging technique outperformed the CS only, however, there were examples where CS only had better performance than averaging; for example, the sensitivity of detecting degenerative change for the “C4/C5” part. Nonetheless, the results demonstrate the promise of the averaging method to accurately detect degenerate change, with over 95% accuracy.

In addition to detecting degenerative change, our method also detects the superior and inferior edges of the vertebral bodies, as shown in Figure 7. While edge detection<sup>15</sup> is not the primary goal of this paper, the



	C1/C2	C2/C3	C3/C4	C4/C5	C5/C6	
Random Forest (averaging)	96.8%	<b>96%</b>	<b>96.1%</b>	<b>95.3%</b>	<b>98%</b>	Accuracy
	<b>100%</b>	<b>100%</b>	<b>100%</b>	98.7%	<b>100%</b>	Sensitivity
	95 %	<b>94.6%</b>	<b>95%</b>	<b>92.4%</b>	<b>97.3%</b>	Specificity
kNN (averaging)	83.9%	84%	82.6%	71.3%	88 %	Accuracy
Random Forest (CS only)	<b>98.6%</b>	94.4%	93.9%	94.2%	96.3%	Accuracy
	<b>100%</b>	96.8 %	94.6%	<b>100%</b>	<b>100%</b>	Sensitivity
	<b>98%</b>	93.5 %	93.6%	88.9%	95.8%	Specificity
kNN (CS only)	86.3%	79.2%	83.4%	80.2%	82.4%	Accuracy

Table 1. Classification performance for detecting degenerative change.

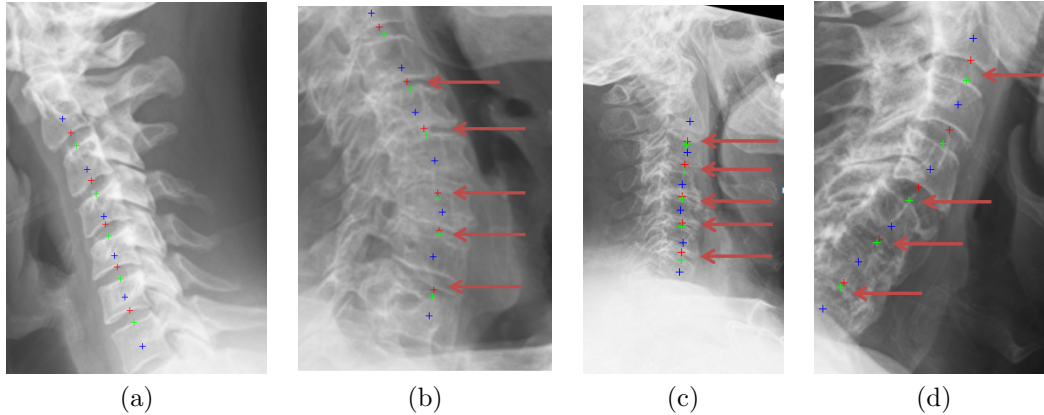


Figure 7. Example results. Detected parts with degenerative change (arrows) along with superior (green) and inferior (red) vertebral body edges.

edges detected by our method could potentially be used in a vertebral body segmentation algorithm. Figure 7 demonstrates example results for four patients. In (a), a patient with no degenerative change is shown, and the approach correctly classifies each part as normal. In (b) and (c), the approach correctly identifies degenerative changes. In (d), the method correctly identifies the degenerative change on the lower portion of the cervical spine, but generates a false positive for C2/C3 near the top of the image.

#### 4. DISCUSSION AND CONCLUSION

Image analysis techniques to analyze the cervical spine often ignore the issue of degenerative change, as radiographs of patients with degenerative change can pose challenges due to the lack of contrast and well defined boundaries at vertebral edges. However, degenerative changes are all too common in patients, particularly in more elderly patients, imaged in routine clinical practice. It is expected that conventional vertebral body segmentation methods<sup>11</sup> that require well defined edges may fail to produce valid results on such patients. Therefore, it is of interest to detect if the patient has degenerative change, and localize the degenerative change in the image. We argue that a robust image analysis technique should be aware of degenerative change in order to produce a robust output. In future work, we are interested to combine the degenerate change detector from this paper with an approach for vertebral body segmentation in the cervical spine.

In this paper we take advantage of the poor edge definition and lack of spacing between vertebrae to capture features correlated with degenerative change, and classify parts of the cervical spine with over 95% accuracy using a Random Forest classifier. These results are encouraging, particularly given the simple input (a small collection of user click points) given to the method. Consequently, the proposed technique is simpler to use than competing methods, and is easily applied to the entire cervical spine. Since much of the processing is done on 1D signals, results are generated quickly.

While the results show much promise, there is room for further work on the problem. First, it would be useful if the method were fully automated. To achieve this, an accurate method to localize the vertebral body centers is required. For patients without degenerative change, this may be possible, although the problem is challenging given the inconsistent number of vertebrae that are imaged in clinical practice. On a diagnostic lateral cervical spine radiograph, all seven cervical vertebral bodies should be visualized, as well as the top of the first thoracic vertebra. However, for some patients, it is difficult to achieve this. Therefore an automated image analysis technique would require robustness to the number of imaged vertebrae, which may be variable. In the case of patients with moderate to severe degenerative change, detecting vertebral body centers is a difficult, open problem.

Another practical challenge is the presence of metal plates, ear rings, and other clutter in the image that may cause the degenerative change detection to fail. Such images were excluded from this study, but a robust solution would ideally be able to handle such cases.

Finally, some degenerative changes cannot be detected solely from the vertebral body region; for example degenerative changes in the spinous processes would be missed by our method; this is also an area of future work.

## ACKNOWLEDGMENTS

This work was supported by the UK Engineering and Physical Sciences Research Council grant number EP/K037641/1.

## REFERENCES

- [1] Cote, P., Cassidy, D. J., and Carroll, L., “The Saskatchewan health and back pain survey: The prevalence of neck pain and related disability in Saskatchewan adults,” *Spine* **23**(15) (1998).
- [2] Todd, A. G., “Cervical spine: Degenerative conditions,” *Current Reviews in Musculoskeletal Medicine* **4**, 168 – 174 (2011).
- [3] Roh, J. S., Teng, A. L., Yoo, J. U., Davis, J., Furey, C., and Bohlman, H. H., “Degenerative disorders of the lumbar and cervical spine,” *Orthopedic Clinics of North America* **36**(3) (2005).
- [4] of Rheumatology, T. D., Medical Illustration, U. o. M., Infirmary, M. R., and the Empire Rheumatism Councils Field Unit, [*The Epidemiology of Chronic Rheumatism*], vol. 2, F.A. Davis Company, Philadelphia PA (1963).
- [5] Frobin, W., Leivseth, G., Biggemann, M., and Brinckmann, P., “Vertebral height, disc height, posteroanterior displacement and dens-atlas gap in the cervical spine: precision measurement protocol and normal data,” *Clinical Biomechanics* **17**(6), 423 – 431 (2002).
- [6] M., C., Stanley, R. J., Long, R., Antani, S., and Thoma, G., “Anterior osteophyte discrimination in lumbar vertebrae using size-invariant features,” *Computerized Medical Imaging and Graphics* **28**, 99 – 108 (2004).
- [7] Abu-Qasmieh, “Multi-class multi-label classification and detection of lumbar intervertebral disc degeneration mr images using decision tree classifiers,” *Computer Engineering and Intelligent Systems* **4**(9) (2013).
- [8] Alomari, R. S., Corso, J. J., Chaudhary, V., and Dhillon, G., “Computer-aided diagnosis of lumbar disc pathology from clinical lower spine mri,” *International Journal of CARS* **5**, 287 – 293 (2010).
- [9] Long, L. R. and Thoma, G. R., “Identification and classification of spine vertebrae by automated methods,” in [*SPIE Medical Imaging*], (2001).
- [10] Chang, Y., Antani, S., Lee, D. J., Gledhill, K., Long, L. R., and Christensen, P., “CBIR of Spine X-ray Images on Inter-vertebral Disc Space and Shape Profiles,” in [*21st IEEE International Symposium on Computer-Based Medical Systems*], (2008).
- [11] Benjelloun, M., Mahmoudi, S., and Lecron, F., “A framework of vertebra segmentation using the active shape model-based approach,” *International Journal of Biomedical Imaging* (2011).
- [12] Centers for Disease Control and Prevention, “Nhanes II project database,” in [<http://archive.nlm.nih.gov/proj/dxpnnet/nhanes/nhanes.php>],
- [13] Chamarty, P., Stanley, R. J., Cizek, G., Long, R., Antani, S., and Thomas, G., “Image analysis techniques for characterizing disc space narrowing in cervical vertebrae interfaces,” *Computerized Medical Imaging and Graphics* **28**(1) (2004).
- [14] Vrtovec, T., Pernus, F., and Likar, B., “A review of methods for quantitative evaluation of spinal curvature,” *European Spine Journal* **18**(5) (2009).
- [15] Lecron, F., Benjelloun, M., and Mahmoudi, S., “Fully Automatic Vertebra Detection in X-Ray Images Based on Multi-Class SVM,” in [*SPIE Medical Imaging: Image Processing*], (2012).